Scripta Materialia 137 (2017) 1–4

Contents lists available at ScienceDirect

Scripta Materialia

journal homepage: www.elsevier.com/locate/scriptamat

Regular article

A robust approach for highly transparent Y_2O_3 ceramics by stabilizing oxygen defects

Wook Ki Jung, Ho Jin Ma, Youngtae Park, Do Kyung Kim *

Department of Materials Science and Engineering, Korea Advanced Institute of Science and Technology (KAIST), 291 Daehak-ro, Yuseong-gu, Daejeon 34141, Republic of Korea

ARTICLE INFO

Article history:
Received 11 March 2017
Accepted 24 April 2017
Available online 1 May 2017

Keywords:
Transparent Y_2O_3 ceramics
Oxygen vacancy
Thermodynamic stabilization
Y_2O_3/ZrO_2 dual powder bed
One-step vacuum sintering

ABSTRACT

Highly transparent Y_2O_3 ceramics were fabricated suppressing the formation of oxygen vacancies during vacuum sintering for the first time. Oxygen stabilization in transparent Y_2O_3 ceramics was successfully enabled by additional ZrO_2 oxygen source considering thermodynamics. The oxygen-stabilized ceramics approached nearly theoretical transmittance without further post-annealing and hot isostatic presssing. This new approach is potentially applicable for the fabrication of other transparent ceramics.

Transparent polycrystalline ceramics have been investigated for infrared (IR) windows, solid-state laser media, scintillators and bio-applications in order to substitute for the single crystals [1–9]. From the perspective of Mie scattering theory, high optical performance of polycrystalline ceramics can be achieved by fabricating pore-free and high purity ceramics [10]. Special sintering technologies such as vacuum sintering, vacuum hot pressing and spark plasma sintering (SPS) are used in order to obtain fully dense ceramics. Sintering in a vacuum condition is widely preferred to remove the nitrogen gas from the pellets [11]. While full density can be obtained via sintering in a vacuum, the final products show black color, or so-called discoloration [12,13]. It is known that the discoloration is due to the oxygen vacancy in the ceramics resulted from the reducing condition in the vacuum. The oxygen vacancies give rise to the formation of F and F^+ centers in the wide band gap and these absorption bands can contribute to the transmission performance below 300 nm [10,14]. It is still unclear what the exact consequences of oxygen vacancies are for larger wavelengths and discoloration.

The oxygen vacancies in the sintered ceramics can be removed conventionally by post-annealing in air or in an oxygen atmosphere [15,16]. However, the post-annealing is insufficient to improve the optical transmittance due to the pore development by evaporation of residual carbon or sulfur particles in the bulk [17,18]. It is difficult to eliminate the oxygen vacancies perfectly preventing the pore development during the post-annealing and the optical performances are inevitably deteriorated. The pore development during the post-annealing inevitably deteriorates the optical performance and therefore, it is difficult to obtain highly transparent ceramics by post-annealing. To solve this problem, the transparent ceramics fabricated via sintering in a vacuum need post-annealing in air for a long time and then further a hot isostatic pressing (HIP) procedure [13,19]. The further HIP process is disadvantageous in the aspect of cost-effectiveness. There is demand to fabricate transparent ceramics via the most simple route possible for the commercialization.

The transparent yttria ceramics has been fabricated recently by one-step vacuum hot pressing employing tantalum foil [20,21]. The green body was wrapped by the tantalum foil to prevent carbon contamination from the graphite mold. The formation of oxygen vacancies also could be restricted to some degree resulting from the low sintering temperature of the hot pressing. The as-sintered samples showed high optical transmittance, but the use of tantalum still has limitations in commercialization considering cost-effectiveness. Wrapping the Y_2O_3 green body with tantalum foil also can cause deformation of the final sintered body including wrinkles.

Herein, we fabricated transparent Y_2O_3 ceramics preventing the formation of oxygen vacancies during the vacuum sintering step. The development of oxygen vacancies was suppressed by thermodynamic stabilization of yttria phase in a vacuum. At elevated temperatures in a vacuum condition, the decrease in oxygen of the yttria powder bed induces oxygen ion diffusion from the pellets to the bed, thereby yielding an undesired oxygen-deficient phase. It was possible to prevent loss of oxygen ions from the pellets using a suitable oxygen supplier considering the thermodynamics. We applied this strategy and successfully fabricated transparent Y_2O_3 ceramics by one-step vacuum sintering for the first time. The as-sintered ceramics showed transmittance that was close to the theoretical value from the visible to the IR range.

* Corresponding author.
E-mail address: dkkim@kaist.ac.kr (D.K. Kim).

http://dx.doi.org/10.1016/j.scriptamat.2017.04.036
1359-6462/

Commercial nano powder Y_2O_3 (99.999%, D_{50} = 50 nm, Lumi M Co Ltd., Seoul, Korea) and $ZrO(CH_2COO)_2$ (Sigma-Aldrich, St. Louis, MO) powders were prepared as raw materials. The raw powders were mixed according to the ZrO_2 doping concentration of 3 mol% and ball milled with ZrO_2 balls in ethanol (99.9%, Samchun, Pyeongtaek, Korea) for 24 h. After ball-milling process, the slurry was dried by hot plate at 80 °C. The dried powder were ground and sieved through a 200-mesh sieve and then calcined at 900 °C for 5 h. The as-calcined powders were uniaxially dry-pressed under 20 MPa into 15 mm diameter steel disks and subsequently were cold isostatically pressed (CIP) under 200 MPa. Sintering was conducted at 2025 K for 5 h in a graphite vacuum furnace. The Y_2O_3 transparent ceramics were mirror-polished on both surfaces. The post-annealing was conducted at temperatures between 1250 and 1450 °C in air for 5 h. The in-line transmittance of the Y_2O_3 ceramics was measured by a UV–Vis-NIR spectrophotometer (Lambda 1050, Perkin Elmer, Wellesley, MA). All the transmittance data were re-calculated to the transmittance at 1 mm thickness. The grain boundaries and pores were observed by transmission electron microscopy (FE-TEM Tecnai G2 F30, FEI Company, Netherlands). The TEM specimens were prepared by a dual beam focused ion beam (DB-FIB, Helios NanoLab, FEI, Netherlands).

The oxygen vacancies are generated in the oxide materials in low oxygen partial pressure at the elevated temperature. An additional source of oxygen is needed to fill the oxygen vacancies [22]. Stabilization of Y_2O_3 is possible by reduction of ZrO_2, which is determined from the Ellingham diagram (Fig. 1(a)) [23]. The oxidation reactions of the Y and Zr are expressed as

$$\frac{4}{3}Y + O_2 \rightarrow \frac{2}{3}Y_2O_3 \quad (1)$$

$$Zr + O_2 \rightarrow ZrO_2 \quad (2)$$

The change of the Gibbs free energy (ΔG_0) of Eqs. (1) and (2) is represented as Eq. (3).

$$\Delta G^0(1) - \Delta G^0(2) < 0 \quad (3)$$

$$\frac{4}{3}Y + ZrO_2 \rightarrow \frac{2}{3}Y_2O_3 + Zr \quad (4)$$

The change of Gibbs free energy is negative (i.e. $-40 <$ kcal/gfw) and Eq. (4) is favored. The Y_2O_3 is thermodynamically stable in contact with the ZrO_2, and the oxygen diffusion could be possible in the Y_2O_3/ZrO_2 interface. The vacuum sintering could be performed at 2025 K in the Y_2O_3-ZrO_2 system considering that the melting points of Zr and ZrO_2 are 2130 K and 2990 K, respectively.

The Y_2O_3 powder bed (Fig. 1(b)), which is conventionally used, is sacrificed to prevent some reduction of the Y_2O_3 pellets. However, at high temperature, oxygen ions are diffused from the Y_2O_3 pellets to the oxygen deficient Y_2O_3 powder bed. The Y_2O_3 pellets suffer oxygen depletion and the oxygen vacancies make the final sintered products darker. To prevent the development of oxygen vacancies in the sintered oxides, oxygen replenishment is needed by supplying an oxygen source. In the Y_2O_3/ZrO_2 dual powder bed (Fig. 1(c)), an additional ZrO_2 layer is used as a source of oxygen. The oxygen vacancies in the Y_2O_3 pellets could be eliminated by oxygen ion diffusion from the ZrO_2 powder, and an oxygen defect-free final product is obtained after sintering in a vacuum. The reduced ZrO_2 powder layer after the vacuum sintering can be easily recycled by heat treatment in air.

Photographs and in-line transmittance of 1-mm thick Y_2O_3 transparent ceramics are presented in Fig. 2(a). The as-sintered body, which is presumed to contain oxygen vacancies, is black and shows decreased overall transmittance. It was also reported that the transparency is extremely deteriorated in all wavelength ranges due to the oxygen-deficient phase in the transparent ceramics [10]. The post-annealing was conducted for the blackish samples to fill the oxygen vacancies. The post-annealing was conducted for the blackish samples to fill the oxygen vacancies. The post-annealed sample shows higher in-line transmittance but a slightly whitish color. A further process such as HIP is needed to obtain nearly theoretical transmittance. In this work, we used the Y_2O_3/ZrO_2 dual powder bed to make oxygen-stabilized Y_2O_3 ceramics for one-step vacuum sintering. The oxygen-stabilized sample shows nearly theoretical transmittance without the post-annealing and HIP procedure. The color of the oxygen-stabilized sample is also very clear as seen by the naked eye. The effects of post-annealing temperature and time on the optical properties of the transparent ceramics have been researched to find the best annealing conditions [12,24]. The post-annealing temperature was changed from 1250 to 1450 °C and all the post-annealed samples were compared with the oxygen-stabilized sample (Fig. 2(b)). The relative in-line transmission at 800 nm was highest in the ceramics post-annealed at 1300 °C (98% @ 800 nm). The oxygen-stabilized specimen shows 99.8% relative in-line transmission at the same wavelength.

The microstructure of the final products was observed to confirm the optical scattering factor in the post-annealed specimen. TEM images of the grain boundary in the transparent Y_2O_3 ceramics are presented in Fig. 3. The as-sintered ceramics for both uncontrolled and oxygen-stabilized specimens are shown in Fig. 3(a) and (c). All the grain boundaries are clean and pore-free. On the other hand, nano pores are observed in the ceramics post-annealed at 1300 °C for 5 h (Fig. 3(b)). The pore size at the grain boundaries is around 23 nm. It is concluded that the grain boundaries include the pores resulting from the post-annealing. A possible reason for pore development during post-annealing has been demonstrated [12,18,25]. The de-sintering phenomenon has been ascribed to minor impurities in the oxide oxidizing and gathering at the grain boundaries in a gas phase. Minor impurities such as carbon or sulfur can be one of the sources of pores, and the preparation of ultra-high purity powder is needed [26,27]. The post-annealing procedure inevitably produces porosity and deteriorates the optical property of transparent ceramics.

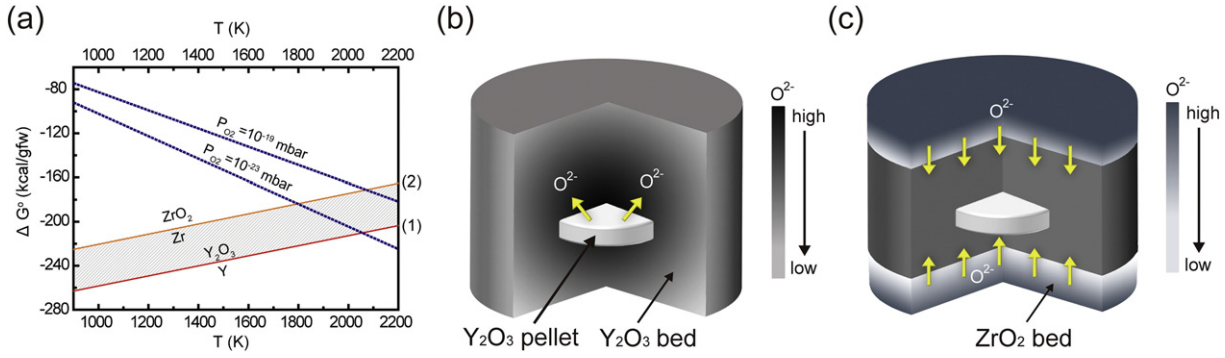

Fig. 1. (a) Ellingham diagram for oxygen reactions at the Y_2O_3/ZrO_2 interface calculated with thermodynamic data [23]. Mechanisms of O^{2-} diffusion during vacuum sintering at 2025 K. (b) Y_2O_3 powder bed; O^{2-} diffusion from the Y_2O_3 pellet to bed. Y_2O_3 pellets suffering for oxygen depletion and metallic during vacuum sintering. (c) Y_2O_3/ZrO_2 dual powder bed; O^{2-} diffusion from additional ZrO_2 layer as an oxygen source.

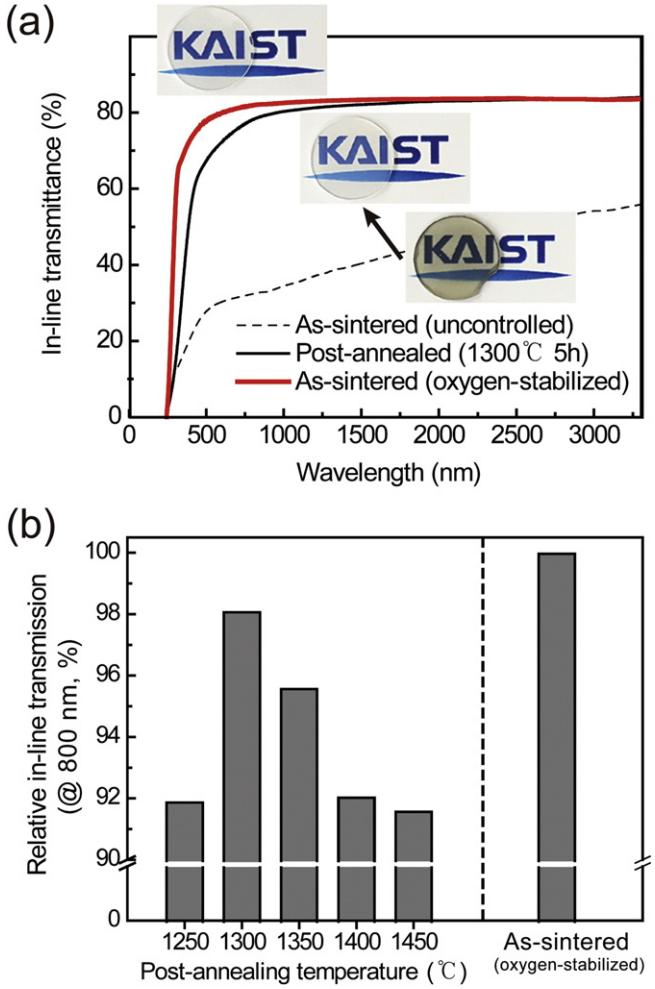

Fig. 2. (a) In-line transmittance of 1 mm-thick Y_2O_3 transparent ceramics. Inset: photographs of the corresponding samples. (b) In-line transmittance evaluated at λ = 800 nm (T_{in}, 800) of the oxygen-stabilized Y_2O_3 ceramics and post-annealed samples from 1250 to 1450 °C for 5 h, respectively.

The origin of the decrease in transmission at the short wavelength region is porosity and it can be demonstrated by the Mie scattering theory. We calculated the estimated size and volume fraction of pores based on the Beer-Lambert law and Mie scattering theory using the in-line transmittance curve of the post-annealed specimen. The Beer-Lambert law can be expressed as Eq. (5), and the surface reflection, R_s is determined by Eq. (6) [28].

$$RIT = (1 - Rs)\ \exp(-\gamma d) \tag{5}$$

$$Rs = \frac{2R'}{1+R'} \quad \text{with } R' = \left(\frac{n-1}{n+1}\right)^2 \tag{6}$$

where R_s is the reflection losses at the two sample surfaces at normal light incidence, and d is the thickness of ceramics. γ describes the total scattering coefficient consisting of grain boundaries, impurities, and pore scattering. The surface reflection is determined by the refractive index n of polycrystalline ceramics, and it is a fundamental physical parameter of materials. The refractive index of Y_2O_3 is given by Eq. (7) [29].

$$n^2 - 1 = \frac{2.578\lambda^2}{\lambda^2 - 0.1387^2} + \frac{3.935\lambda^2}{\lambda^2 - 22.936^2} \tag{7}$$

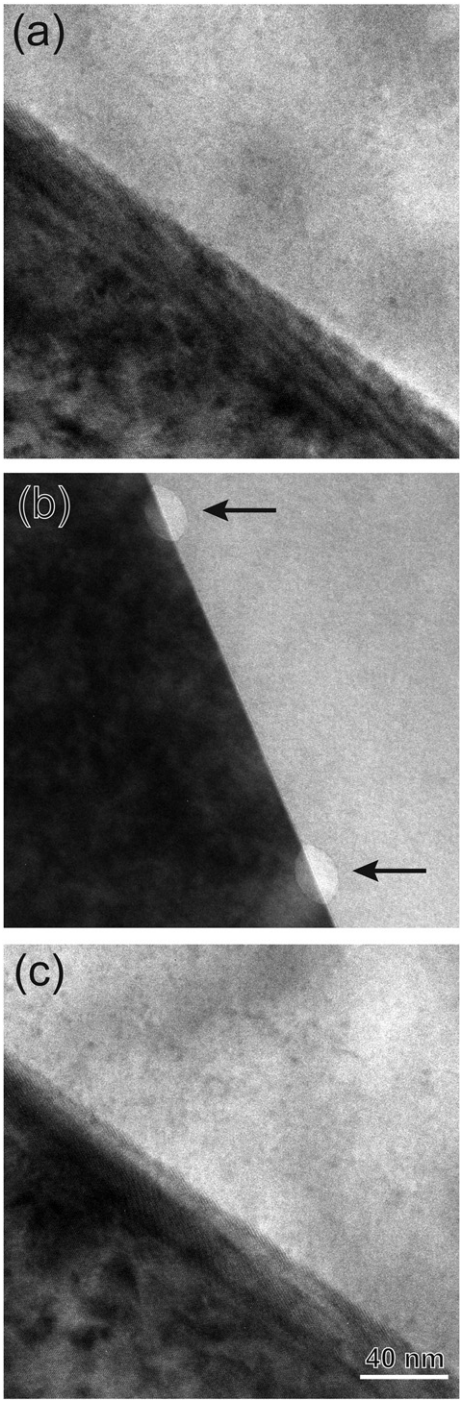

Fig. 3. (a) TEM images of the grain boundary microstructure in transparent Y_2O_3 ceramics. (a) As-sintered ceramics (uncontrolled). (b) Post-annealed one at 1300 °C for 5 h; nano pores at the grain boundaries indicated by the black arrows. (c) As-sintered ceramics (oxygen-stabilized).

The scattering coefficient of porosity, γ_{pore} can be expressed as Eq. (8) [28,30].

$$\gamma_{pore} = \frac{p}{(4/3)\pi r^3} \cdot C_{Sca,pore} \tag{8}$$

where p is the total porosity, r is the pore radius, and $C_{sca,pore}$ is the scattering cross-section of one spherical pore. The $C_{sca,pore}$ can be derived

from the Mie solution to the Maxwell equation. The specific calculation was conducted using the computation code [31]. Here, we assumed that the pore size is bimodal and follows a Zero-Order Lognormal Distribution (ZOLD). The ZOLD distribution function, f(r), is expressed as Eq. (9) [32].

$$f(r) = k \exp\left\{\frac{[\log(r) - \log(r_m)]^2}{2s^2}\right\} \quad (9)$$

where k is the normalization factor, r_m is the most frequent radius, and s is the distribution width. Curve fitting was attempted to obtain the maximum R square value, R_2.

As shown in Fig. 4(a), the calculated transmittance curve shows good agreement with the measured value when assuming the pores have a bimodal distribution ($R_2 > 99\%$). The calculated radius, r_m, is around 8 and 20 nm, respectively. The calculated ZOLD distributions of the pore radius are also represented in Fig. 4(b). The estimated pore radius is very similar with the observed value at the grain boundaries. It is determined that the post-annealing can deteriorate the transmission of transparent Y_2O_3 ceramics because of the development of pores at the grain boundaries. Further study of the origin of pore development in transparent Y_2O_3 ceramics is needed.

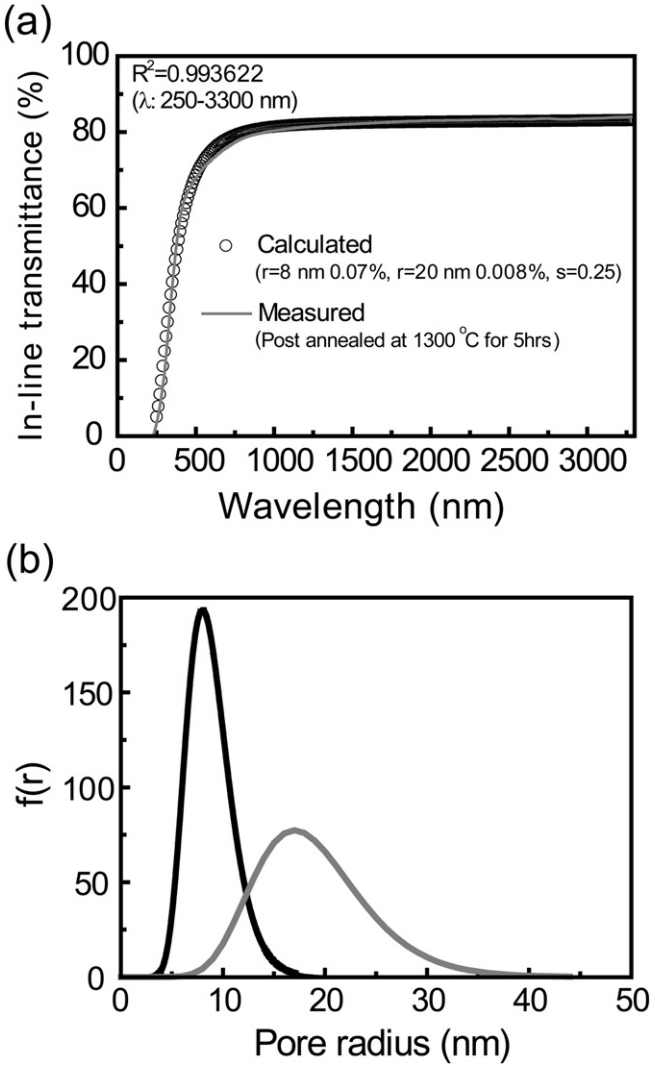

Fig. 4. (a) Calculated pore size and distribution based on the measured transmittance data of the post-annealed one at 1300 °C for 5 h. The solid curve; measured transmittance. The circles; calculated transmittance assuming that bimodal pore size and ZOLD distribution by using Mie scattering theory. (b) Semi-logarithmic plot of ZOLD distributions, f(r) versus pore radius.

In conclusion, the suppression of the oxygen vacancies during the fabrication of transparent ceramics is demonstrated successfully by introducing a Y_2O_3/ZrO_2 dual powder bed, considering the thermodynamics. The problem of oxygen depletion in the Y_2O_3 pellets can be solved by utilizing an additional ZrO_2 powder layer as an oxygen supplier. The one-step vacuum sintering is a powerful method enabling facile, cost-effective fabrication and high in-line transmittance of the as-sintered transparent ceramics. This concept is potentially applicable for the fabrication of other transparent oxides.

Acknowledgements

This work was supported by the Materials & Components Technology Development (MCTD) Program (Project no. 10047010) funded by the Ministry of Trade, Industry & Energy (MOTIE) of Korea.

References

[1] S.F. Wang, J. Zhang, D.W. Luo, F. Gu, D.Y. Tang, Z.L. Dong, G.E.B. Tan, W.X. Que, T.S. Zhang, S. Li, L.B. Kong, Prog. Solid State Chem. 41 (2013) 20–54.
[2] J. Sanghera, W. Kim, G. Villalobos, B. Shaw, C. Baker, J. Frantz, B. Sadowski, I. Aggarwal, Materials 5 (2012) 258–277.
[3] Y. Damestani, C.L. Reynolds, J. Szu, M.S. Hsu, Y. Kodera, D.K. Binder, B.H. Park, J.E. Garay, M.P. Rao, G. Aguilar, Nanomed. Nanotechnol. Biol. Med. 9 (2013) 1135–1138.
[4] W.K. Jung, H.J. Ma, S.W. Jung and D.K. Kim, J. Am. Ceram. Soc., online published, http://dx.doi.org/10.1111/jace.14776.
[5] A. Ikesue, Y.L. Aung, Nat. Photonics 2 (2008) 721–727.
[6] Y.K. Kim, H.K. Kim, G. Cho, D.K. Kim, Nucl. Instrum. Methods Phys. Res., Sect. B 225 (2004) 392–396.
[7] Y.K. Kim, H.K. Kim, D.K. Kim, G. Cho, J. Mater. Res. 19 (2004) 413–416.
[8] Y. Li, Y. Wu, J. Am. Ceram. Soc. 98 (2015) 2972–2975.
[9] P. Zhang, P. Liu, Y. Sun, X. Peng, Z. Wang, S. Wang, J. Zhang, J. Alloys Compd. 657 (2016) 246–249.
[10] A. Krell, J. Klimke, T. Hutzler, Opt. Mater. 31 (2009) 1144–1150.
[11] Y. Huang, D. Jiang, J. Zhang, Q. Lin, Z. Huang, J. Am. Ceram. Soc. 93 (2010) 2964–2967.
[12] G. Spina, G. Bonnefont, P. Palmero, G. Fantozzi, J. Chevalier, L. Montanaro, J. Eur. Ceram. Soc. 32 (2012) 2957–2964.
[13] W. Zhang, T. Lu, B. Ma, N. Wei, Z. Lu, F. Li, Y. Guan, X. Chen, W. Liu, L. Qi, Opt. Mater. 35 (2013) 2405–2410.
[14] V.T. Gritsyna, I.V. Afanasyev-charkin, V.A. Kobyakov, K.E. Sickafus, J. Am. Ceram. Soc. 73 (1999) 3365–3373.
[15] W. Zhang, T. Lu, N. Wei, B. Ma, F. Li, Z. Lu, J. Qi, Opt. Mater. 34 (2012) 685–690.
[16] L. An, A. Ito, T. Goto, J. Am. Ceram. Soc. 94 (2011) 3851–3855.
[17] I. Reimanis, H.J. Kleebe, J. Am. Ceram. Soc. 92 (2009) 1472–1480.
[18] K. Morita, B.N. Kim, H. Yoshida, K. Hiraga, Y. Sakka, J. Eur. Ceram. Soc. 36 (2016) 2961–2968.
[19] W. Zhang, T. Lu, N. Wei, B. Ma, F. Li, Z. Lu, J. Qi, Opt. Mater. 34 (2012) 685–690.
[20] L. Gan, Y.-J. Park, M.-J. Park, H. Kim, J.-M. Kim, J.-W. Ko, J.-W. Lee, J. Am. Ceram. Soc. 98 (2015) 2002–2004.
[21] L. Gan, Y. Park, H. Kim, J. Kim, J. Ko, J. Lee, J. Eur. Ceram. Soc. Ceram. Soc. 36 (2016) 911–916.
[22] T. Gerber, P. Lömker, B. Zijlstra, C. Besson, D. Müller, W. Zander, J. Schubert, M. Gorgoi, M. Müller, J. Mater. Chem. C (2016) 1813–1820.
[23] H.J.T. Ellingham, J. Soc. Chem. Ind. Lond. 63 (1944) 125.
[24] K. Morita, B.-N. Kim, H. Yoshida, K. Hiraga, Y. Sakka, Acta Mater. 84 (2015) 9–19.
[25] H. Zhang, B.N. Kim, K. Morita, H. Yoshida, J.H. Lim, K. Hiraga, J. Am. Ceram. Soc. 94 (2011) 2981–2986.
[26] J. Sanghera, S. Bayya, G. Villalobos, W. Kim, J. Frantz, B. Shaw, B. Sadowski, R. Miklos, C. Baker, M. Hunt, I. Aggarwal, F. Kung, D. Reicher, S. Peplinski, A. Ogloza, P. Langston, C. Lamar, P. Varmette, M. Dubinskiy, L. Desandre, Opt. Mater. 33 (2011) 511–518.
[27] W. Kim, G. Villalobos, C. Baker, J. Frantz, B. Shaw, S. Bayya, B. Sadowski, M. Hunt, I. Aggarwal, J. Sanghera, Opt. Eng. 52 (2012) 21003.
[28] R. Apetz, M.P.B. Van Bruggen, J. Am. Ceram. Soc. 86 (2003) 480–486.
[29] Y. Nigara, Jpn. J. Appl. Phys. 7 (1968) 404–408.
[30] M. Stuer, P. Bowen, M. Cantoni, C. Pecharroman, Z. Zhao, Adv. Funct. Mater. 22 (2012) 2303–2309.
[31] C. Mätzler, IAP Res. Rep. 8 (2002) 1–24.
[32] B.D. William, W. Chen, J. Am. Ceram. Soc. 76 (1993) 2086–2092.